

Alpha-Smooth Muscle Actin Expression and Parafoveal Blood Flow Pathways Are Altered in Preclinical Diabetic Retinopathy

Dong An,^{1,2} Jonathan Chung-Wah-Cheong,¹ Dao-Yi Yu,^{1,2} and Chandrakumar Balaratnasingam¹⁻³

¹Lions Eye Institute, Nedlands, Western Australia, Australia

²Centre for Ophthalmology and Visual Science, University of Western Australia, Perth, Western Australia, Australia

³Department of Ophthalmology, Sir Charles Gairdner Hospital, Nedlands, Western Australia, Australia

Correspondence: Chandrakumar Balaratnasingam, Lions Eye Institute, 2 Verdun Street, Nedlands, WA 6009, Australia; balaratnasingam@gmail.com.

DA and JC contributed equally to the work presented here and should therefore be regarded as equivalent first authors.

Received: October 4, 2021

Accepted: April 22, 2022

Published: May 6, 2022

Citation: An D, Chung-Wah-Cheong J, Yu D-Y, Balaratnasingam C. Alpha-smooth muscle actin expression and parafoveal blood flow pathways are altered in preclinical diabetic retinopathy. *Invest Ophthalmol Vis Sci.* 2022;63(5):8. <https://doi.org/10.1167/iovs.63.5.8>

PURPOSE. To investigate differences in alpha smooth muscle actin (α SMA) expression and parafoveal blood flow pathways in diabetic retinopathy (DR).

METHODS. Human donor eyes from healthy subjects ($n = 8$), patients with diabetes but no DR (DR-; $n = 7$), and patients with clinical DR (DR+; $n = 13$) were perfusion labeled with antibodies targeting α SMA, lectin, collagen IV, and filamentous actin. High-resolution confocal scanning laser microscopy was used to quantify α SMA staining and capillary density in the parafoveal circulation. Quantitative analyses of connections between retinal arteries and veins within the superficial vascular plexus (SVP), intermediate capillary plexus (ICP) and deep capillary plexus (DCP) were performed.

RESULTS. Mean age between the groups was not different ($P = 0.979$). α SMA staining was seen in the SVP and ICP of all groups. The DCP was predominantly devoid of α SMA staining in control eyes but increased in a disease stage-specific manner in the DR- and DR+ groups. The increase in α SMA staining was localized to pericytes and endothelia of terminal arterioles and adjacent capillary segments. Capillary density was less in the DCP in the DR+ group ($P < 0.001$). ICP of the DR- and DR+ groups received more direct arteriole supplies than the control group ($P < 0.001$). Venous outflow pathways were not altered (all $P > 0.284$).

CONCLUSIONS. Alterations in α SMA and vascular inflow pathways in preclinical DR suggest that perfusion abnormalities precede structural vascular changes such as capillary loss. Preclinical DR may be characterized by a “steal” phenomenon where blood flow is preferentially diverted from the SVP to the ICP and DCP.

Keywords: retina, macula microvasculature, capillary, smooth muscle actin/ α SMA, diabetic retinopathy

Diabetic retinopathy (DR) is a progressive disorder of the retinal vasculature than can lead to severe vision loss.¹⁻³ Early detection and intervention of retinal vascular dysregulation are a key strategy in mitigating irreversible neuronal injury in diabetes.⁴ The retinal microaneurysm is defined as the earliest clinical manifestation of DR⁵; however, histologic studies have shown that irreversible endothelia injury and pericyte loss have already occurred prior to the formation of microaneurysms.^{1,6} The pathophysiological mechanisms underlying the earliest stages of DR before the occurrence of permanent cellular injury such as those seen in microaneurysms are less clear. Several proposed mechanisms of microaneurysm formation include vascular stasis,⁷ fat emboli,⁸ varicose formation,⁹ and pericyte loss leading to structural weakness.¹⁰ A greater understanding of these mechanisms is important, as it will serve to prevent vision loss in diabetes by facilitating earlier intervention.

Oxygen consumption in the retina, per gram tissue, is greater than that in most other organs in the human body.¹¹ Blood flow to various vascular layers of the macula are constantly fluctuating in order to maintain the dynamic balance between energy supply and demand.¹²⁻¹⁴ Blood flow is regulated by key elements of the vascular apparatus, including pericytes, endothelia, and smooth muscle cells.¹⁵⁻¹⁸ Alpha smooth muscle actin (α SMA) is a filamentous contractile protein that is ubiquitously distributed throughout the vascular system and contributes to the control of vascular diameter, vascular tone, and retinal blood flow.^{17,19,20} In the brain, disease-induced alterations in the contractile elements of the vascular tree are inherently linked to the pathogenesis of major neurological diseases.²¹ Such changes can alter regional perfusion patterns and initiate or propagate neuronal injury. There is clinical and experimental evidence to implicate retinal perfusion abnormalities in patients with diabetes.²²⁻²⁴ These observations may

be explained by significant alterations to the contractile elements of the retinal vascular tree that control perfusion.

The organization of the macular circulation is highly specialized.^{25,26} In a recent study, we showed that there is great variation in the distribution of α SMA contractile proteins between parafoveal capillary beds, suggesting that the characteristics of physiologic perfusion and vulnerability to vascular injury may vary between retinal layers.²⁵ The purpose of this report is to define disease stage-specific changes to contractile proteins, arterial inflow pathways, and venous outflow pathways within the parafovea in eyes of donors with diabetes. We performed a detailed histologic study that included eyes from donors without diabetes, donors with diabetes but without clinical manifestations of DR,⁵ and donors with DR. The results were used to hypothesize the pattern of microregional blood flow changes due to diabetes and their chronologic relationship to the onset of structural clinical changes such as capillary loss and microaneurysms.²⁷ This report expands our understanding of the pathophysiology of DR and provides novel insights into how macula perfusion with respect to vascular topology might be disturbed in the earliest stages of DR.

MATERIALS AND METHODS

The study was approved by the human research ethics committee at the University of Western Australia. All human tissue was handled according to the tenets of the Declaration of Helsinki.

Donor Eyes and Assignment of Groups

The donor cohort was stratified into three groups: control group, diabetes without retinopathy group (DR-), and diabetes with retinopathy group (DR+). The control group was comprised of eyes with no history of retinal disease and no history of diabetes mellitus. The DR- and DR+ groups were comprised of eyes from donors that upon medical record review were confirmed to have a diagnosis of diabetes mellitus and were treated with an oral antiglycemic agent and/or insulin. On microscopic examination, eyes that demonstrated any histologic vascular alterations that characterize DR, including microaneurysms, capillary non-perfusion,²⁷ retinal hemorrhage, and intraretinal microvascular abnormalities, were assigned to the DR+ group (Supplementary Figs. S1, S2).^{7,8} Eyes from donors with diabetes mellitus that did not demonstrate any features of DR were assigned to the DR- group. Additionally, 15 donor eyes were not studied due to postmortem tissue changes. These were excluded from the study. Postmortem tissue changes include significant loss of retinal integrity resulting in tears and breakdown and any significant clots detected within the vasculature resulting in absent or reduced perfusion downstream that is not part of DR pathology (Supplementary Fig. S3).

Donor Retina Preparation

Human donor eyes used in this report were obtained from DonateLife WA, the organ and tissue retrieval authority in Western Australia, Australia, and the Lions Eye Bank. Eyes were enucleated within 24 hours of death and prepared using our previously described techniques.^{25,28,29} No primary antibody control was utilized to test non-specific binding of secondary antibodies. No secondary antibody control was utilized to detect autofluorescence among

the protein targets of interest. In brief, enucleated eyes were transported in oxygenated Ringer's lactate solution and were then placed in a custom-built eye holder. The central retinal artery was cannulated for perfusion labeling using a glass micropipette (100- μ m tip diameter) and perfused with the following solutions in sequence at a rate of 60 μ L/min unless otherwise stated: 1% bovine serum albumin in Ringer's solution for 20 minutes to wash out blood clots; 4% paraformaldehyde in 0.1-M phosphate buffer (PB) for 20 minutes; and 0.1-M PB for 20 minutes. Next, eyes were perfused using one or more of the following protocols (Table 1):

- Lectin—Lectin—fluorescein isothiocyanate (FITC; 40 μ g, L4895; Sigma-Aldrich, St. Louis, MO, USA) and Hoechst stain (2.5 μ L; H6024; Sigma-Aldrich) in 400 μ L PB were perfused over a period of 30 seconds, stained for 12 minutes, and washed out using PB over 20 minutes. Lectin binds to the glycoproteins of endothelial cell membrane.³⁰
- Filamentous actin (F-actin)/phalloidin—Triton X-100 (0.1%; Sigma-Aldrich) in 0.1-M PB was perfused for 5 minutes, followed by 1 μ g phalloidin tetramethylrhodamine B isothiocyanate (phalloidin-TRITC, P1951; Sigma-Aldrich) and Hoechst stain (2.5 μ L in 1 mL PB) delivered over three 30-second perfusions 20 minutes apart, and then washed out using PB over 20 minutes. F-actin is found in cellular cytoskeleton and is most abundant in vascular smooth muscle cells.²⁰
- Collagen IV—Triton X-100 (0.1%) in 0.1-M PB was perfused for 5 minutes, followed by 10 μ g rabbit anti-collagen IV antibodies (SAB4300738; Sigma-Aldrich), 10 μ L 100% goat serum, and Hoechst stain (2.5 μ L in 1 mL PB) delivered over three 30-second perfusions, each 20 minutes apart, and then washed out with PB perfusion over 20 minutes after a total of 1 hour of labeling time. Next, 20 μ L of goat anti-rabbit (Alexa Fluor 488, ab150077; Abcam, Cambridge, UK) in 1 mL PB was delivered via three 30-second perfusions, each 20 minutes apart, followed by washout using PB after 1 hour. Collagen IV is a structural protein of basement membrane that is present throughout the vasculature.³¹ This procedure allows for clear visualization of vascular structures in diabetic retina without obscuration from label leakage that is sometimes seen in lectin and phalloidin labeling. Due to collagen IV having autofluorescence properties within the ultraviolet and blue spectrum, negative control was not performed, and secondary antibodies targeting this spectrum were avoided.
- α SMA—Triton X-100 (0.1%) in 0.1-M PB was perfused for 5 minutes followed by 20 μ L mouse anti- α SMA antibodies (A2547; Sigma-Aldrich) and 10 μ L 100% donkey serum in 1 mL PB delivered via three 30-second perfusions, each 20 minutes apart, then washed out using PB after a total of 1 hour of labeling time. Next, 20 μ L of donkey anti-mouse (Alexa Fluor 647, ab150111; Abcam) in 1 mL PB was delivered via three 30-second perfusions, each 20 minutes apart, and washed out using PB after 1 hour of labeling time. α SMA is most abundant in smooth muscle cells and endothelium of small arteries and arterioles within the retinal microvasculature.²⁰ It has also been

TABLE 1. Donor Demographic Information and Staining Protocols

Eye	Group	Age (y)	Sex	Cause of Death	αSMA	Collagen IV	Lectin	F-Actin
1	Control	18	M	Drug overdose	✓			✓
2	Control	86	F	CVA	✓	✓	✓	
3	Control	86	F	CVA	✓	✓	✓	
4	Control	63	F	Septic arthritis			✓	✓
5	Control	46	M	Angiosarcoma	✓			✓
6	Control	46	M	Angiosarcoma	✓			✓
7	Control	72	F	Endometrial Ca	✓		✓	
8	Control	72	F	Endometrial Ca	✓		✓	
9	DR-	66	M	CVA	✓			✓
10	DR-	55	F	Renal cell Ca	✓	✓	✓	
11	DR-	74	M	Trauma				✓
12	DR-	73	M	AMI	✓			✓
13	DR-	58	F	AMI				✓
14	DR-	60	F	Endometrial Ca	✓			✓
15	DR-	54	M	Pituitary adenoma			✓	
16	DR+	50	M	Renal cell Ca	✓			✓
17	DR+	50	M	Renal cell Ca	✓			✓
18	DR+	70	M	Cardiomyopathy		✓		✓
19	DR+	70	M	Cardiomyopathy		✓	✓	
20	DR+	59	M	AMI	✓	✓		✓
21	DR+	58	M	Acute pancreatitis	✓			✓
22	DR+	58	M	Acute pancreatitis	✓			✓
23	DR+	82	M	AMI			✓	
24	DR+	82	M	AMI			✓	
25	DR+	66	M	AMI			✓	
26	DR+	70	M	DM complications				✓
27	DR+	70	M	DM complications				✓
28	DR+	45	F	DM complications				✓

CVA, cerebral vascular accident; Ca, carcinoma; AMI, acute myocardial infarction; DM, Diabetes mellitus. Eyes 2/3, 5/6, 7/8, 16/17, 18/19, 21/22, 23/24, and 26/27 were pairs of donor eyes belonging to the same donor.

used as a pericyte marker.³²⁻³⁵ The efficacy of αSMA labeling of pericytes is illustrated in Supplementary Figure S4.

Post-perfusion, eyes were decannulated and dissected along the equator. Vitreous was carefully peeled and dissected from the retina. The posterior segment was then immersed in 4% paraformaldehyde for 12 hours. Next, the neuroretina was detached from the retinal pigment epithelium. The optic nerve head was sectioned to be continuous with the retina. The retina was flatmounted on a glass slide by making several radial incisions along the edge. Glycerol (Merck Australia, Bayswater, Victoria, Australia) was added to enhance the optical quality of the tissue before placement of the coverslip.

Confocal Scanning Laser Microscopy

A confocal scanning laser microscope (Eclipse 90i and C1; Nikon Corporation, Tokyo, Japan) equipped with four solid-state lasers at wavelengths of 405, 488, 561, and 635 nm was used to scan flatmounted retina samples. For each retina sample, a whole-retina montage (NIS Elements; Nikon Corporation) was created using low-magnification images acquired with a Nikon 4×, numerical aperture (NA) 0.20 dry objective lens (Supplementary Figs. S1, S2). Next, an image with a field of view of 3.64 × 3.64 mm, centered on the fovea, was acquired by digitally stitching nine 1.27 × 1.27-mm images together, in a 3 × 3 configuration with 5% overlap using a Nikon 10× NA 0.45 dry objective lens. Z-stacks were imaged by taking optical sections of the sample 1 μm

apart between the inner limiting membrane and the outer nuclear layer. Out of the nine imaged areas for each macula, the superior, inferior, nasal, and temporal stacks (Supplementary Fig. S5) were utilized to measure capillary density and to study vessel branching patterns.

High-magnification images were acquired from each αSMA and F-actin co-labeled retina using a Nikon 40× oil NA 1.3× objective lens with a field of view of 0.31 × 0.31 mm. Image stacks with optical sections 0.5 μm apart were acquired to visualize endothelial cells, pericytes, and precise locations of αSMA staining. Immunofluorescence labeling using Hoechst (405 nm), lectin-FITC (488 nm), phalloidin-TRITC (561 nm), and Alexa Fluor donkey anti-mouse (635 nm) were visualized via argon laser excitation with emissions detected through 450-, 561-, 605-, and 668-nm bandpass filters, respectively.

Image Analysis

Confocal image files were processed with IMARIS v7.4.2 (Bitplane, Zurich, Switzerland) and/or ImageJ (National Institutes of Health, Bethesda, MD, USA). Figures were compiled with Illustrator CC 25.4.1 (Adobe, San Jose, CA).

Stratification of Macula Microvasculature Plexuses. The macula circulation was stratified into the superficial vascular plexus (SVP), which is between the inner limiting membrane and the ganglion cell layer/inner plexiform layer border; the intermediate capillary plexus (ICP), which is located in the inner half of the inner nuclear layer; and the deep capillary plexus (DCP), which is located between the outer half of the inner nuclear layer and the

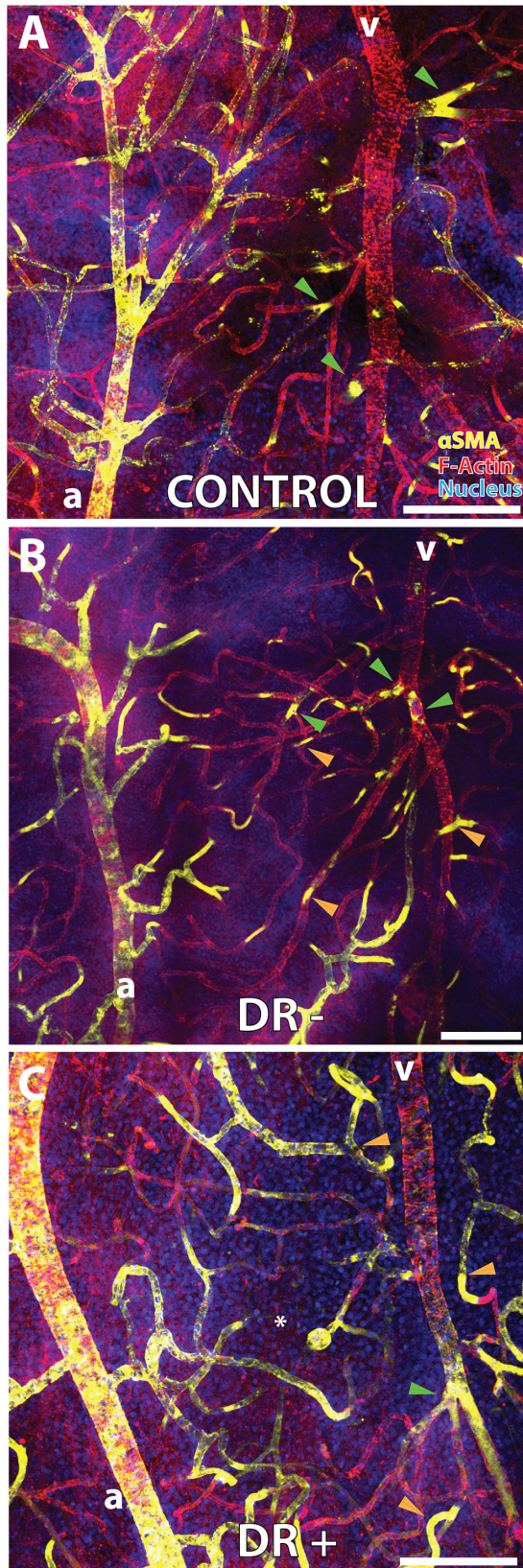


FIGURE 1. Comparison of α SMA staining distribution between an artery (*a*) and a vein (*v*) across the control group (A), DR- group (B), and DR+ group (C). Strong α SMA staining of the artery, arterioles, and capillaries adjacent to the artery was observed for all three groups. In the control group, α SMA staining was largely devoid from venules but demonstrated strong staining at venular junction sites

outer plexiform layer (OPL).^{25,26} Co-localization to nuclear label was used to stratify each plexus. Two-dimensional (2D) images were generated by projecting all confocal slices that comprised a single capillary plexus (using the 10 \times lens) and were used to attain quantitative measurements.

Grading of α SMA-Labeled Images. SVP, ICP, and DCP images from all donors were randomized (JC) and presented to two masked graders (DA, CB). The graders were instructed to grade each image as α SMA-label “positive” or “negative.” The result was used as a reliability index for qualitative analysis of α SMA staining. Qualitative analyses were performed for patterns of α SMA staining distribution along sections of retinal microvasculature. Quantitative image intensity measurements were not performed due to the following two factors: (1) retinas of different natural thickness result in variable depth of each plexus, thus requiring variable laser power for capture; and (2) the degree of diabetic retinal edema alters the vascular plexus depth and laser power required for capture. This variation occurs within retinal eccentricities and between individuals. The most representative images of α SMA distribution along retinal microvasculature were selected to study qualitatively.

Capillary Density Measurements. Images (1.27 \times 1.27 mm) acquired from the superior, inferior, nasal, and temporal regions of the perifovea were used to quantify capillary densities of SVP, ICP, and DCP of each group. Using our previously published methods,^{26,36–38} a 3 \times 3 grid was drawn on each of the 2D images, and the number of capillaries intersected by the grids were manually counted to represent the relative capillary density in this field (Supplementary Fig. S5B).

Vessel Order Definitions. The current study utilized the Horton–Strahler³⁹ nomenclature (Supplementary Fig. S6) to assign vessel orders, which was utilized in our previous report.²⁵ In brief, the system starts at the capillary level and proceeds centripetally. The order is increased if two segments of equal order join at a junction. Capillary is designated as *c*, pre-capillary arteriole as *a1*, and venule formed by adjoining capillaries as *v1*. In our previous report, we concluded, based on vessel tracing, that the retinal artery that branches from the artery of the arcade and courses toward the fovea is order *a4*.²⁵ Arterioles that branch from *a4* to supply the retinal plexuses are order *a3*. Large venules that drain a plexus into the SVP are *v3*, and the retinal veins located within the SVP are *v4*.²⁵

Arterial Inflow Analysis. Arterial inflow pathways were analyzed based on our previously published methods.²⁵ Criteria for differentiating retinal artery, arterioles, capillaries, venules, and veins were reported in detail within our previously published report.²⁵ In brief, the IMARIS Surpass function was used to visualize the retinal vasculature at different angles of rotation to define inflow and outflow

(green arrows). In the DR- group, additional α SMA staining was observed at venular junctions (green arrows) and in some short capillary segments (orange arrows). In the DR+ group, significantly more α SMA staining was found on the venous aspect of the vasculature. Some capillaries had more α SMA staining across an entire segment (orange arrows). Significantly more α SMA staining was seen along the distal portion of the vein and all of its tributaries (green arrow). A microaneurysm was seen adjacent to an area of capillary non-perfusion (white asterisk). α SMA, F-actin, and nucleus were false-colored yellow, red, and blue, respectively. All images are to the same scale. Scale bars: 150 μ m.

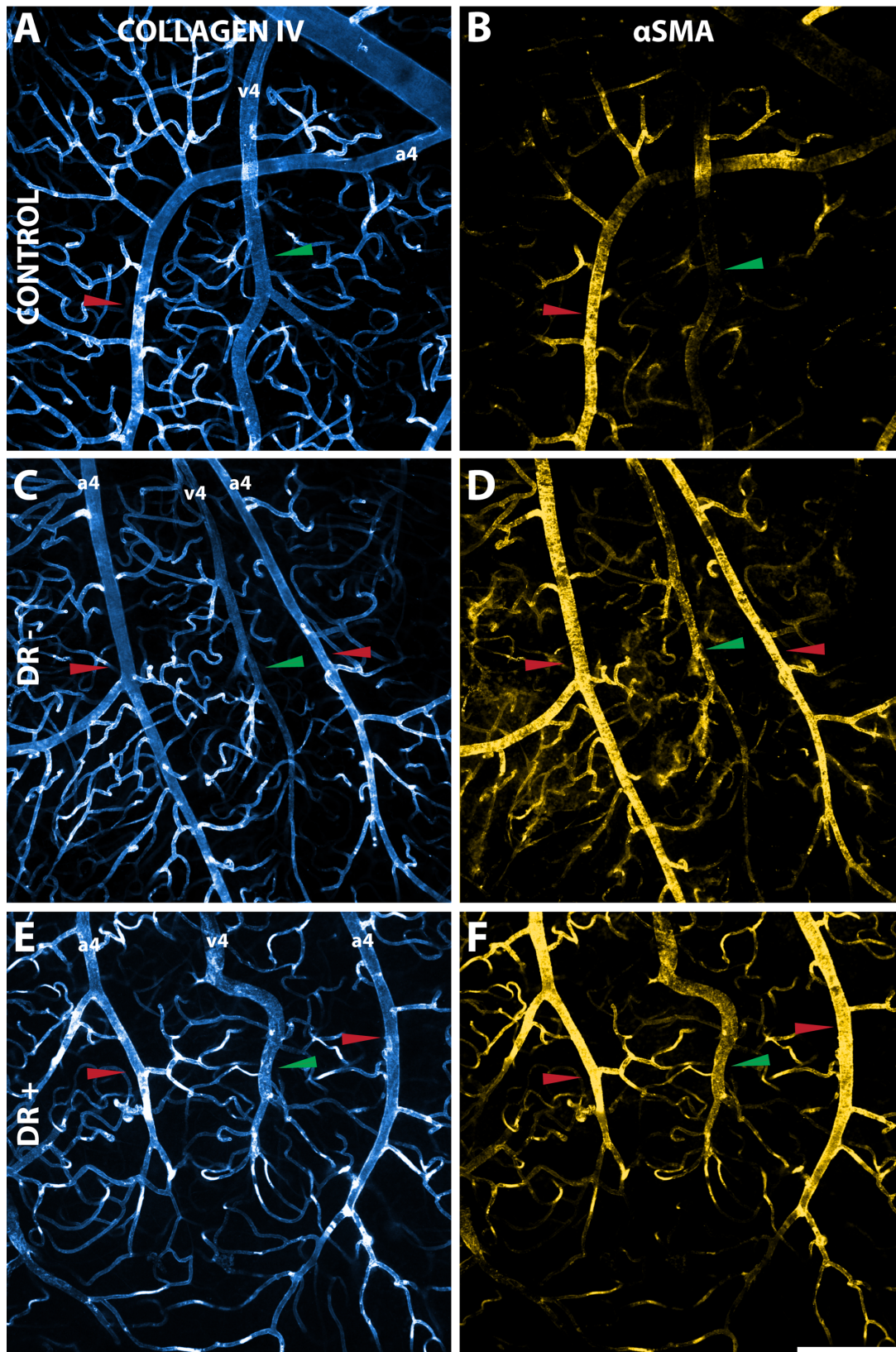


FIGURE 2. Comparisons of the superficial vascular plexus among the control group (A, B), DR- group (C, D), and DR+ group (E, F). All images were acquired from within the macula region, superior to the fovea. The *left panel* contains images with collagen IV staining, and the *right panel* contains the same images with α SMA staining. Consistent staining patterns were observed for collagen IV across the three groups, where all orders of vessels demonstrated similar staining intensities. The *a4* and *v4* vessels are indicated on the collagen IV panel. For α SMA staining, retinal veins from both the DR- and DR+ groups demonstrated stronger staining compared to the control group. Arteries are indicated by *red arrows* and veins by *green arrows* in both panels. All images are to the same scale. *Scale bar:* 300 μ m.

TABLE 2. Analysis of Capillary Density Count Using ANOVA

	Capillary Density			P		
	Control	DR-	DR+	Control vs. DR-	Control vs. DR+	DR- vs. DR+
SVP	40.4 ± 10.8	46.6 ± 13.1	47.1 ± 12.0	0.350	0.293	0.898
ICP	46.2 ± 11.4	46.8 ± 13.3	48.1 ± 13.2	0.968	0.927	0.882
DCP	36.9 ± 8.2	41.1 ± 17.6	20.4 ± 18.6	0.309	<0.001	<0.001

pathways. Inflow pathways were studied to determine connections among arteries, arterioles, and capillaries. An *a4* retinal artery was identified, and all of its tributary *a3* arterioles were traced to the plexus that they first supply. The proportions of *a3* arterioles that supply each plexus was statistically compared between each group. Individual arterioles were then traced until they reached the DCP via connecting vessels.

Venous Outflow Analysis. A *v4* retinal vein located within the SVP was first identified. All of its tributaries (*v3*) were manually traced retrogradely into their respective plexus of origin. The total number of *v3* was recorded for each plexus. The proportion of *v3* for each plexus was calculated and compared among each of the three groups.

Statistical Analysis

Data were analyzed using SigmaPlot 12.0 (SYSTAT Software, Chicago, IL) and R (R Foundation for Statistical Computing, Vienna, Austria). One-way ANOVA was used to compare age among the groups. Two-way ANOVA was used to compare capillary densities within and between each group and each vascular plexus. For inflow and outflow branching pathway analysis, the proportions of each branching pathway were compared among groups using one-way ANOVA. $P \leq 0.050$ was considered significant. Results are presented as mean ± standard deviation.

RESULTS

General

Twenty-eight eyes from 20 donors were used in this study. After microscopic examination, eight eyes from five donors were assigned to the control group, seven eyes from seven donors were assigned to the DR- group, and 13 eyes from eight donors were assigned to the DR+ group. Detailed donor demographic information and immunohistochemical labeling protocols can be found in Table 1. Mean ages of the control group (57.0 ± 26.2 years), DR- group (62.9 ± 8.3 years), and DR + group (62.5 ± 12.0 years) were similar ($P = 0.979$).

Heterogeneous αSMA Staining Between Retinal Artery and Vein

Representative full-projection images of parafoveal vasculature in each group are provided in Figure 1. In the control group, vessels on the arterial aspect demonstrated strong αSMA staining, and vessels on the venous aspect demonstrated weaker or no αSMA staining (Fig. 1A). An exception was that veins and venules showed strong αSMA staining at junctions where two or more venules converged (Fig. 1A). In the DR- group, more αSMA staining was found on the venous aspect of the vasculature. Compared to the control

group, in the DR- group there was also more αSMA staining outside of venular junctional zones (Fig. 1B). In the DR+ group, significant numbers of venules and capillaries were found to have more αSMA staining adjacent to retinal veins (Fig. 1C).

Staining Patterns of Retinal Vascular Plexuses

Superficial Vascular Plexus. All orders of retinal vasculature demonstrated complete labeling of collagen IV across the control, DR-, and DR+ groups (Figs. 2A, 2C, 2E). Arteries, arterioles, capillaries, venules, and veins demonstrated similar levels of collagen IV stain intensity. Arteries and arterioles demonstrated strong αSMA staining across the groups (Figs. 2B, 2D, 2F). There was more αSMA staining in both the DR- and DR+ groups in veins and capillaries compared to the control group (Figs. 2B, 2D, 2F). Capillary density for the SVP was similar across all three groups (all $P > 0.050$) (Table 2).

Intermediate Capillary Plexus. Collagen IV staining demonstrated a similar intensity of staining for all groups (Figs. 3A, 3C, 3E). Microaneurysms in the DR+ group appeared brightly hyperfluorescent with collagen IV stain (Fig. 3E). Compared to the control group, αSMA staining was stronger in the DR- group (Figs. 3B, 3D). In DR+ group, there was evidence of significantly more αSMA staining in some capillary segments (Fig. 3F). Capillary density for the ICP was similar across all three groups (all $P > 0.050$) (Table 2).

Deep Capillary Plexus. Collagen IV stain demonstrated complete DCP labeling for both the control and DR- groups (Figs. 4A, 4C). Microaneurysms and sites of capillary nonperfusion were clearly identified in the DR+ group (Fig. 4E). There was minimal αSMA staining within the DCP of the control group (Fig. 4B). The DR- group demonstrated segmental hyperfluorescence of αSMA staining along the vascular course (Fig. 4D). The DR+ group demonstrated significantly more αSMA staining compared to both groups, with many long segments of capillaries displaying hyperfluorescence (Fig. 4F). DCP capillary density of the DR+ group was significantly less compared to both the control and DR- groups (both $P < 0.001$).

Endothelial Cells and Pericytes of the Deep Capillary Plexus. All orders of DCP vasculature, including *a1*, capillaries, and venules, stained positively for F-actin in the DCP across the three groups (Figs. 1, 5). In the control group, the *a1* arteriole segment, which connects the ICP and DCP as the terminal arteriole, consisted of both pericytes and endothelial cells that expressed αSMA (Figs. 5B, 5C, 5D). Endothelial cells and pericytes of capillaries beyond the *a1* inflow sites were found not to express any αSMA (Figs. 5E, 5F). Compared to controls, all eyes in the DR- group showed more capillary αSMA staining in the DCP within close vicinity of the *a1* inflow site. An example is provided in Figure 6. Both endothelial cells and pericytes

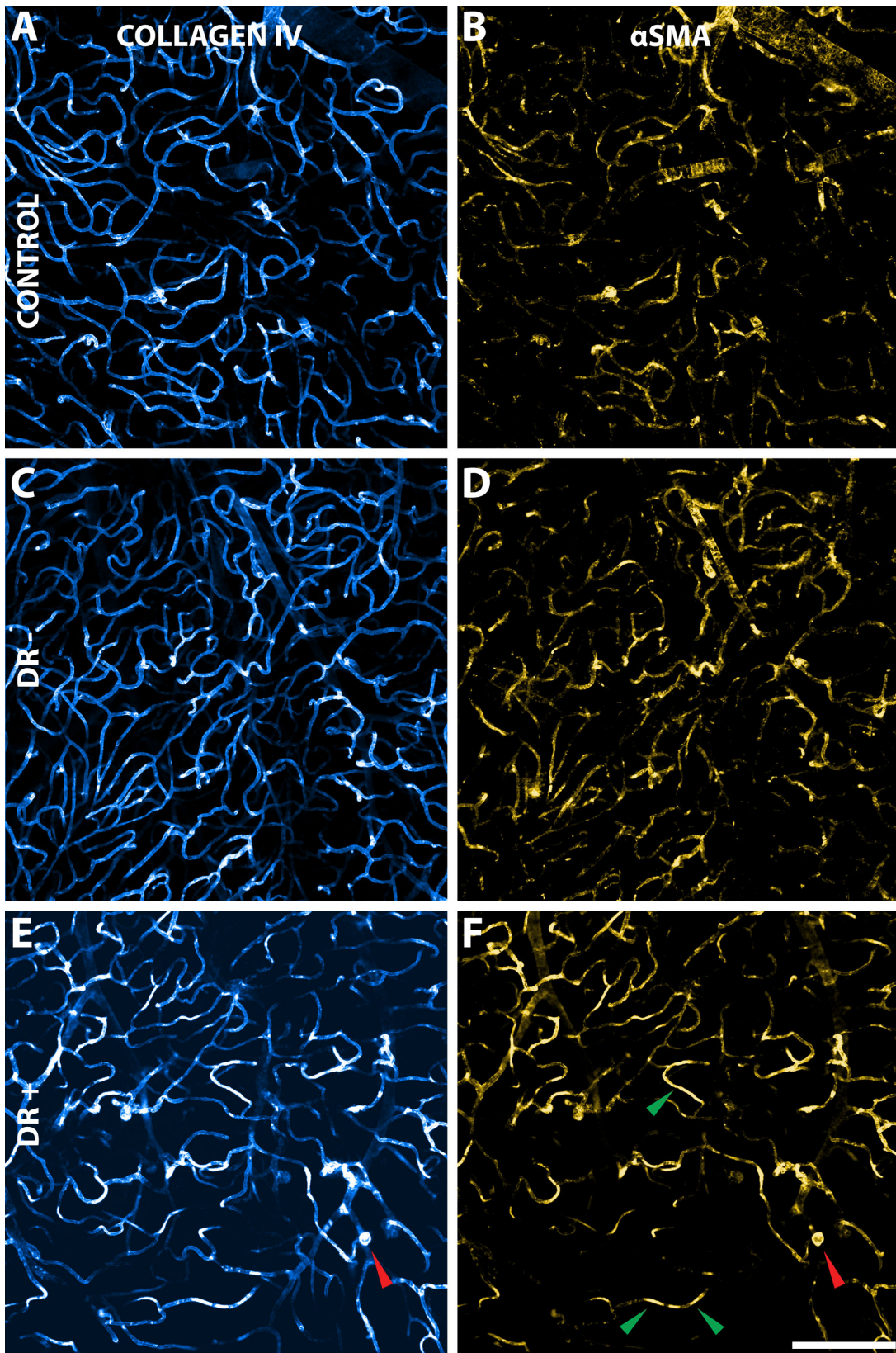


FIGURE 3. Comparisons of the intermediate capillary plexus among the control group (A, B), DR- group (C, D), and DR+ group (E, F). The left panel contains images with collagen IV staining, and the right panel contains the same images with α SMA staining. Collagen IV staining patterns were similar between the control and DR- groups. In the DR+ group, a microaneurysm can be seen (red arrow). There was more α SMA staining in the DR- and DR+ groups compared to the control group. Many capillaries of the DR+ group appeared hyperfluorescent (green arrows). All images are to the same scale. Scale bar: 300 μ m.

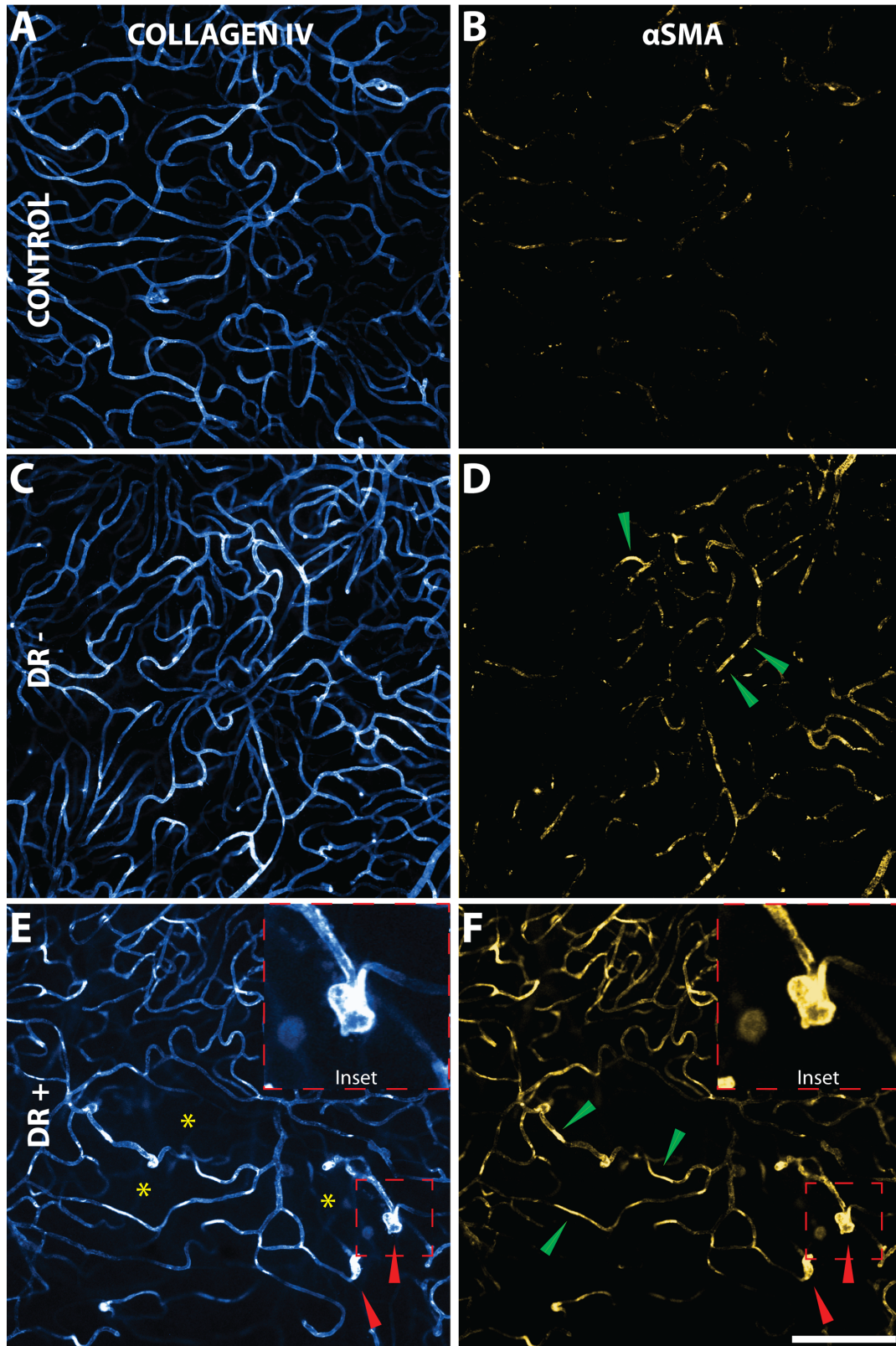


FIGURE 4. Comparisons of the deep capillary plexus among the control group (**A, B**), DR- group (**C, D**), and DR+ group (**E, F**). The left panel contains images with collagen IV staining, and the right panel contains the same images with α SMA staining. Collagen IV staining patterns were similar between the control and DR- groups. The DR+ group demonstrated several capillary non-perfusion sites (yellow asterisks) and microaneurysms (red arrows). Levels of α SMA staining across the three groups differed, as minimal α SMA staining was seen in the control group (**B**), but more α SMA staining was found in the DR- group. There was evidence of focal hyperfluorescence of capillary segments (**D**; green arrows). The DR+ group showed significantly more α SMA staining, with many capillary segments showing hyperfluorescence (**F**; green arrows). The microaneurysm seen in the DR+ panel is highlighted in an inset. All images are to the same scale. Scale bar: 300 μ m.

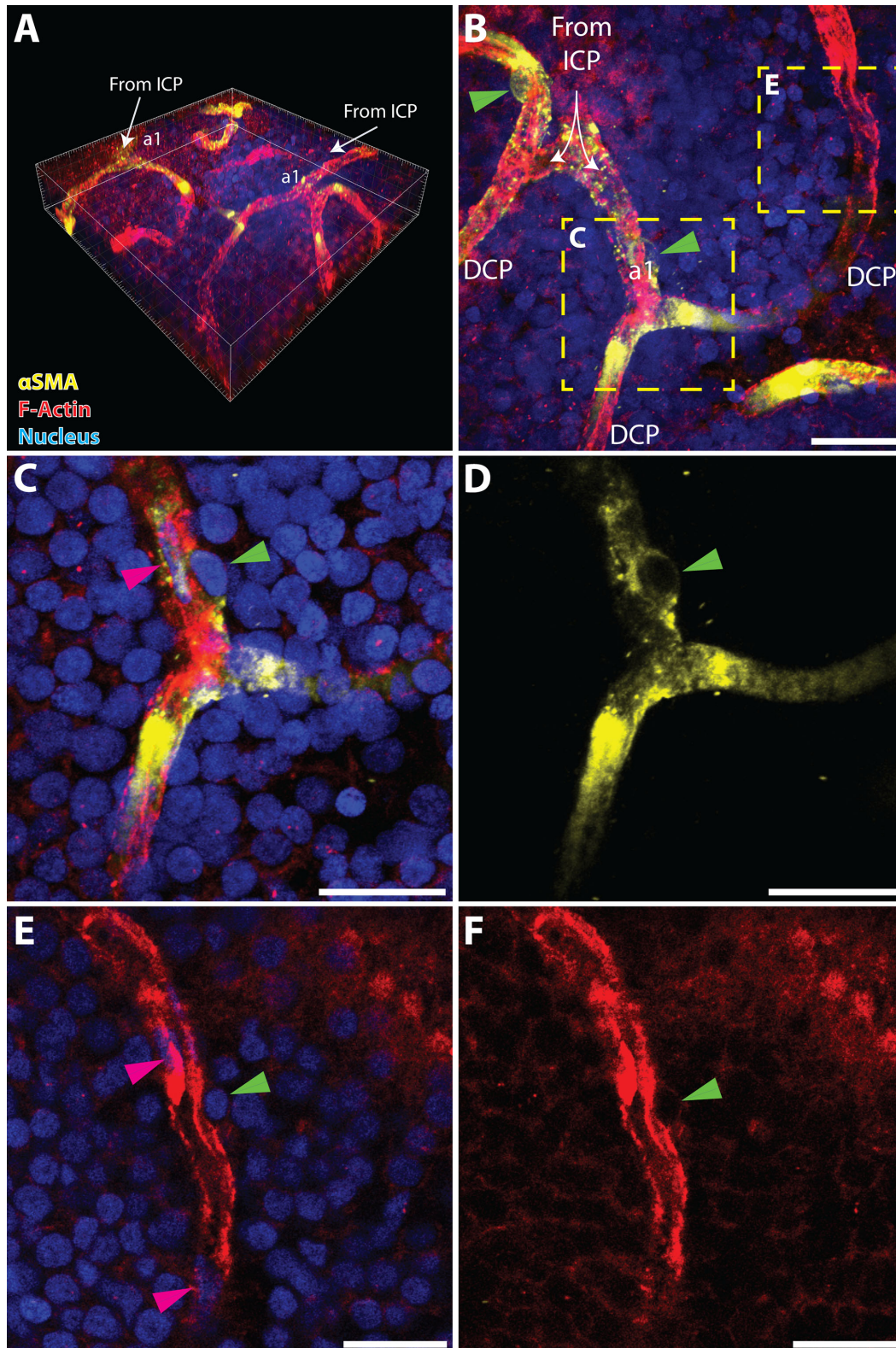


FIGURE 5. Illustration of α SMA staining patterns of the DCP in the control group using three-dimensional (3D) high-resolution microscopy. (A) The 3D stack shows the connections patterns between the ICP and the DCP via pre-capillary arterioles designated as *a1*. (B) The projected view of all slices illustrates the sites of α SMA termination as *a1* enters the DCP; pericytes that expressed α SMA can be seen along the *a1* (green arrow). (C) The spatial relationship between an endothelial cell and the pericyte along *a1*. (D) α SMA expression by the pericyte. (E, F) Endothelial cells of the more distal segment of DCP capillary did not express α SMA (magenta arrows). The pericyte also did not express α SMA (green arrows). α SMA, F-actin, and nucleus were false-colored yellow, red, and blue, respectively. Scale bars: 30 μ m.

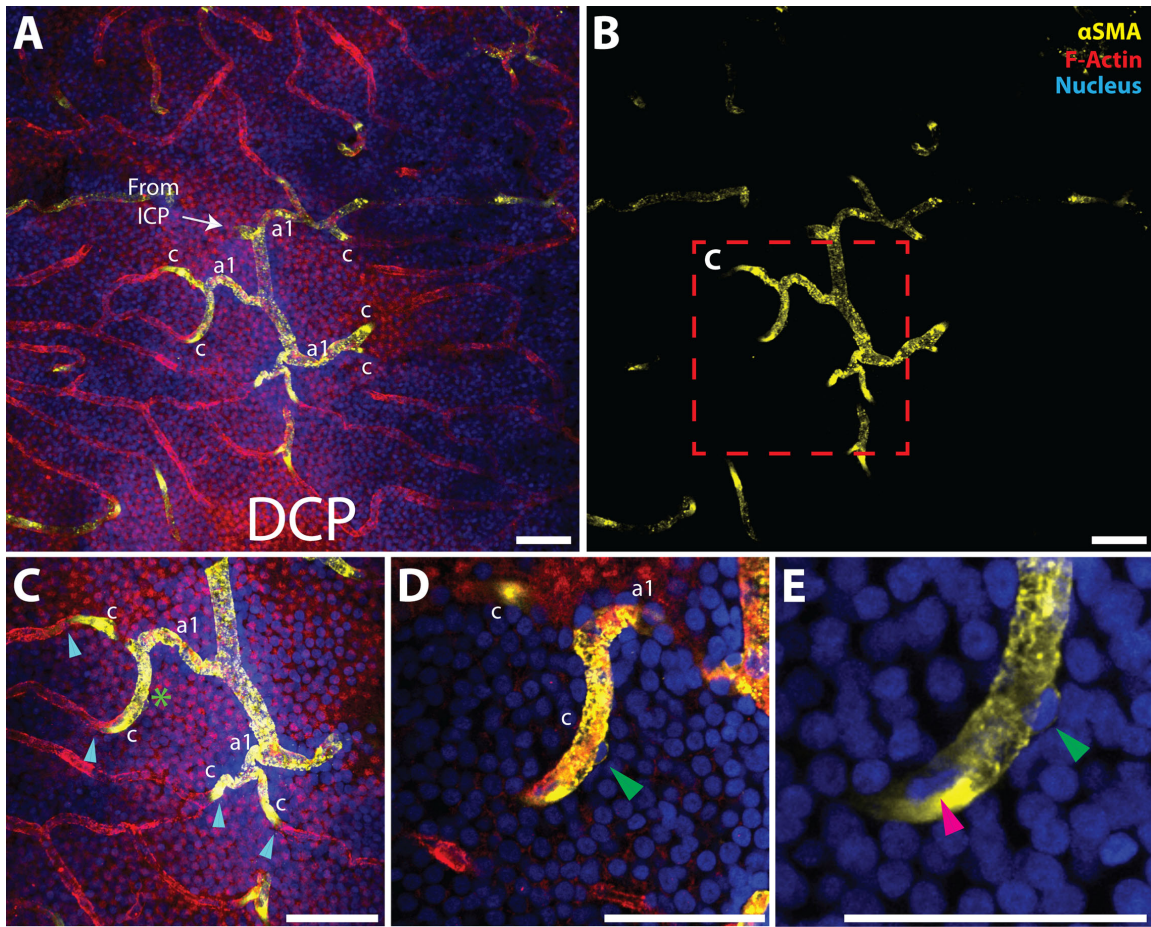


FIGURE 6. α SMA staining patterns of the DCP in the DR- group. (A, B) α SMA staining can be seen within *a1* and the proximal segment of capillary (*c*) downstream of *a1*. (C) The transition sites of α SMA expression/non-expression within DCP capillaries are indicated by *blue arrows*; panel C is an inset of A and B. (D) A capillary segment of interest is marked by a *green asterisk*. A pericyte that expressed α SMA is indicated by a *green arrow*. (E) Magnified view of this pericyte, as well as an α SMA-expressing endothelial cell (*magenta arrow* indicates an elongated cell nucleus). Beyond this endothelial cell, the capillary no longer expressed α SMA. α SMA, F-actin, and nucleus were false-colored *yellow, red, and blue*, respectively. Scale bars: 100 μ m.

in this region expressed α SMA (Figs. 6D, 6E). In the DR+ group, additional α SMA staining was found in the DCP both

downstream of *a1* and at venular junctions adjacent to *v3* (Fig. 7). Some distal capillary segments of the DCP away

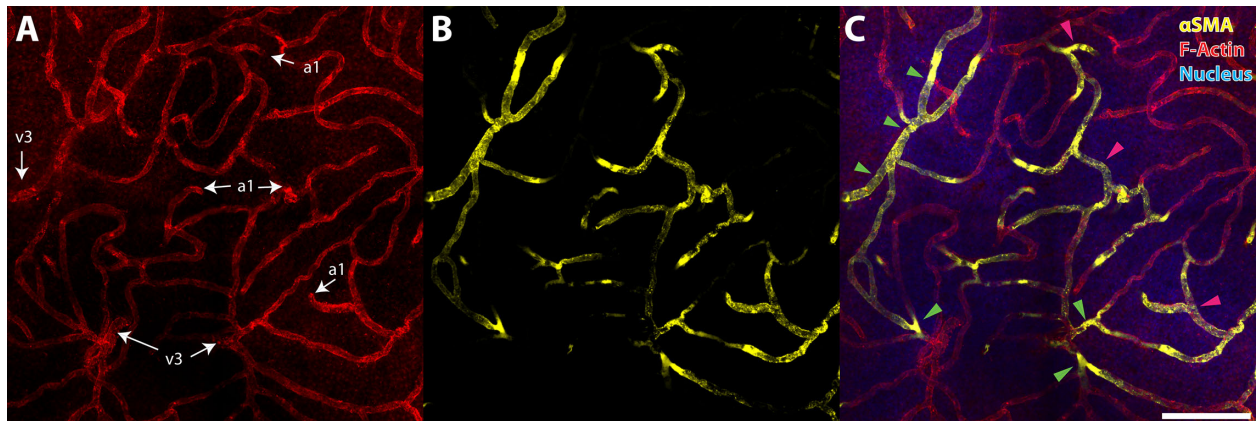


FIGURE 7. α SMA staining patterns of the DCP in the DR+ group. (A) The points of inflow (*a1*) and outflow (*v3*) are marked on a DCP section labeled with F-actin. (B) There was significantly increased α SMA staining in the DCP. (C) Sites of increased α SMA staining included capillary segments adjacent to *a1* (*magenta arrows*) and *v3* (*green arrows*). α SMA, F-actin, and nucleus were false-colored *yellow, red, and blue*, respectively. Scale bar: 150 μ m.

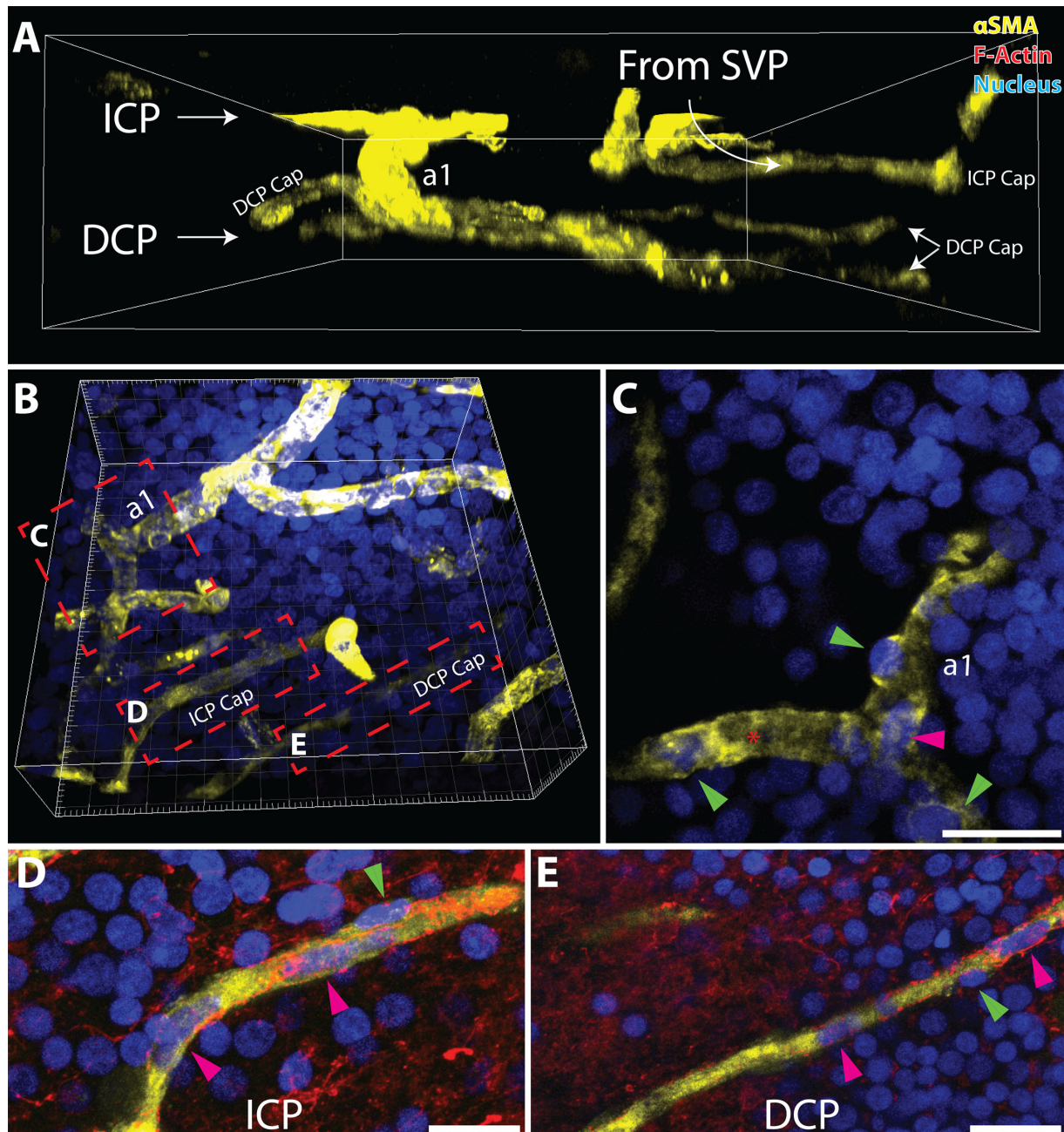


FIGURE 8. Illustration of α SMA staining pattern of the DCP in the DR+ group. (A) A 3D stack was rotated and visualized through the x,z -axis to highlight the connection between the ICP and DCP via the $a1$ arteriole. (B) Segments of both the ICP and DCP capillaries (Cap); the 3D stack was also viewed through the x,y -axis. The three insets highlight (C) a $a1$ bifurcation site, (D) an ICP capillary, and (E) a distal segment of DCP capillary. All three capillary segments were found to have α SMA-expressing pericytes (green arrows) and endothelial cells (magenta arrows). In addition, the capillary at the $a1$ bifurcation was found to have an enlarged diameter (11.5 μ m; red asterisk). α SMA, F-actin, and nucleus were false-colored yellow, red, and blue, respectively. Scale bars: 30 μ m.

from inflow and outflow sites were also found to have α SMA staining (Fig. 8). Their endothelial cells and pericytes both expressed α SMA (Fig. 8D), but this was not observed in the other groups (Figs. 5, 6).

Vascular Branching Analysis

Inflow Pathway Analysis. In the control group, 150 $a3$ arterioles were identified; 167 were identified from the DR- group and 172 from the DR+ group. In the control

group, 79.3% of arterioles first supplied the SVP. Numerous connecting vessels were found between the SVP and ICP; 20.7% of arterioles directly supplied the ICP, bypassing the SVP. There was no evidence of direct arteriolar supply to the DCP from an $a4$ artery. Arteriolar supply to the DCP was via $a1$ vessels originating from the ICP. In the DR- group, 52.7% of arterioles supplied the SVP and 47.3% supplied directly to the ICP. In the DR+ group, 51.7% of arterioles supplied the SVP and 48.3% supplied directly to the ICP. Similar to the controls, both DR- and DR+ groups had no

TABLE 3. Summary of Inflow and Outflow Pathway Analyses

	Inflow Pathway Analysis, $\alpha 3$ Arteriole			Outflow Pathway Analysis, $v 3$ Venule			
	N	SVP-ICP-DCP, % (n)	ICP-DCP, % (n)	N	SVP, % (n)	ICP, % (n)	DCP, % (n)
Control	150	79.3 (119)	20.7 (31)	518	42.2 (219)	34.9 (181)	22.7 (118)
DR-	167	52.7 (88)	47.3 (79)	865	42.4 (367)	35.1 (304)	22.4 (194)
DR+	172	51.7 (89)	48.3 (83)	1004	41.3 (415)	36.3 (365)	22.3 (224)

Sample sizes of $\alpha 3$ arterioles and $v 3$ venules are indicated in parentheses. Inflow pathway indicates the course that the $\alpha 3$ arteriole took to reach the deep plexus. Outflow pathway indicates the plexus of origin of the $v 3$ venule.

direct arteriolar supply to the DCP from the $\alpha 4$ artery. Both groups had significantly lower SVP arteriole proportions and higher ICP arteriole proportions compared to the control group (both $P < 0.001$) (Table 3).

Outflow Pathway Analysis. In the control group, 518 $v 3$ venules were identified; 42.2% of these originated from the SVP, 34.9% from the ICP, and 22.7% from the DCP. In the DR- group, 865 $v 3$ venules were identified; 42.4% of these originated from the SVP, 35.1% from the ICP, and 22.4% from the DCP. In the DR+ group, 1004 $v 3$ venules were identified; 41.3% of these originated from the SVP, 36.3% from the ICP, and 22.3% from the DCP. There was no difference in venular outflow pathway proportions for the SVP ($P = 0.638$), ICP ($P = 0.284$), or DCP ($P = 0.818$) across the three groups (Table 3).

DISCUSSION

The purpose of this study was to define stage-specific changes to vascular α SMA expression and macula blood flow pathways in DR. As it is difficult to perform in vivo imaging of human retinal capillary blood flow, we used three-dimensional quantitative structural data of the vascular network to infer knowledge regarding macula perfusion alterations in the different stages of DR. Our findings suggest that micro-regional blood flow changes precede clinically detectable retinal structural alterations in DR^{5,7,40}; therefore, detection of such changes could serve as a surrogate marker of early vascular dysregulation in diabetes.

The energy required to support neuronal and glial function is immense but also highly varied between retinal layers.^{14,41,42} Accordingly, the morphology and spatial organization of the macula circulation demonstrates regional specializations that reflect the unique energy requirements of each retinal layer.^{25,43} As the extent of neural activity is rapidly and constantly fluctuating, vascular specializations are also required to facilitate precise temporal modulation of retinal blood flow.^{20,43} α SMA is a filamentous protein that confers contractile properties to cells and thereby regulates regional blood flow by controlling vascular diameter and resistance.^{19,34,44} In our previous reports we defined the topographic distribution of α SMA in the healthy human macula and demonstrated non-uniform distribution among the superficial, intermediate, and deep capillary plexuses.^{20,25} One of the most interesting findings was the relative paucity of α SMA in the capillaries of the deep plexus and the abrupt termination of α SMA staining in $\alpha 1$ arterioles that connect the ICP to the DCP.²⁵ This particular pattern of α SMA distribution has also been described in cortical networks of the brain where α SMA termini are commonly seen in second-order arterioles and represent the boundary between ensheathing and mesh pericytes.⁴⁵ Because mesh pericytes of the brain have a limited capacity to regulate

blood flow, it is proposed that they have a significantly lower expression of α SMA.

In this report, we have demonstrated that the pattern of α SMA expression is altered in the earliest stages of DR before the onset of clinically visible structural changes such as microaneurysms. Specifically, there was more α SMA expression in the capillaries of the ICP and DCP in the DR- group compared to controls. A stage-specific increase in α SMA expression continued to occur in the ICP and DCP following the onset of clinical DR, such as the loss of capillaries and appearance of microaneurysms. There is some overlap in the physiologic properties of retinal and cortical vascular networks. In the brain, one of the most reliable means of determining if vessels less than 10 μ m in diameter have contractile properties is to assess the magnitude of α SMA expression.^{46,47} Another important property of human vascular networks is that they can acquire contractile properties de novo in pathologic states by increasing α SMA expression.⁴⁸ As an example, following experimental cardiac ischemia, pericytes near blockage sites can adapt contractile characteristics by increasing α SMA expression.⁴⁸ Similarly, in the brain following ischemic stroke, persistent pericyte-mediated contraction marked by elevated α SMA expression has been found to inhibit capillary re-perfusion.²¹ In this study, we found that higher expression of α SMA was localized to both pericytes and endothelia, providing evidence that perfusion abnormalities in DR may be regulated by numerous elements of the vascular system and not just pericytes. Alterations in α SMA expression may influence vascular resistance³⁹ and hemorheologic properties such as red blood cell deformability and adherence.⁴⁹ Such changes may in turn alter regional oxygen handling and exchange by RBCs.

Retinal blood flow is dynamic, and regional perfusion is coordinated by numerous checkpoints within the vascular tree.⁴³ Kornfield and Newman¹⁷ used flicker stimulation to study blood flow regulation in the rodent retinal circulation with several important findings. First, they found that functional hyperemia in the retina is driven principally by the active dilation of arterioles. They also demonstrated differential regulation of blood flow between the capillary plexuses. Finally, they demonstrated a correlation between the amount of α SMA expression and the degree of vascular contractility. The marked alterations in α SMA staining demonstrated in this study suggest that the control points for blood flow may be modified in DR. Although α SMA expression was higher in the DCP, closer observation revealed that the pattern of additional α SMA staining was not diffuse but rather localized to capillaries in close proximity to $\alpha 1$ and $v 3$ segments. This study was not designed to determine the etiology of the localized α SMA changes in the DCP, but we speculate that it may represent critical sites where endothelial wall shear stress patterns are altered due to vascular bifurcation or the presence of hemodynamic gradients.⁵⁰ Functional

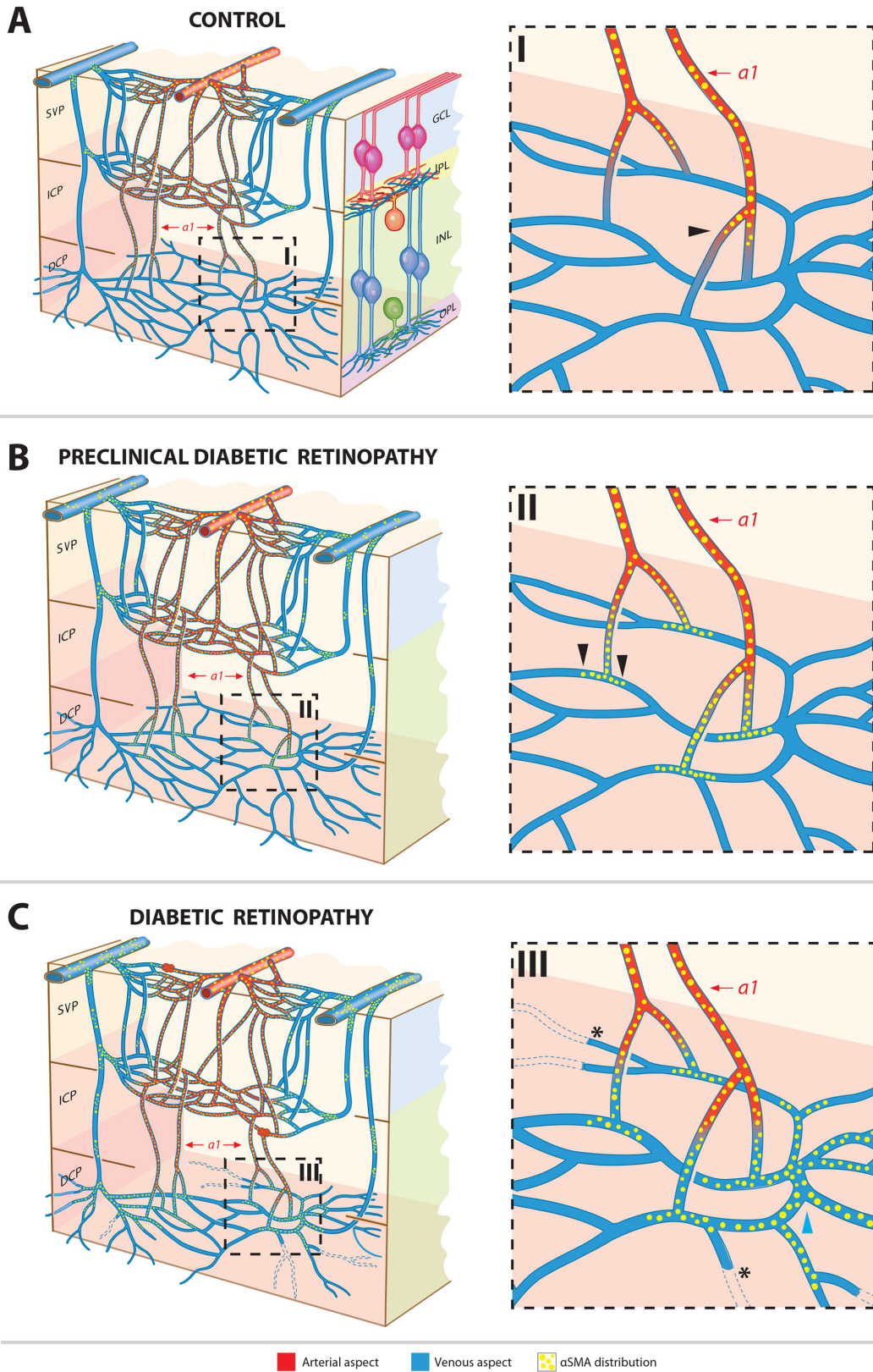


FIGURE 9. Schematic representation of α SMA distribution and changes in the development of diabetic retinopathy. Insets provide magnified views of regions of interest. **(A)** In the control group, α SMA (yellow dots) was predominantly localized within arteries, arterioles, and capillaries on the arterial aspect of the circulation (red). For the venous aspect (blue), α SMA was localized to major venular junctions only. Within the connecting arterioles (*a1*) between the ICP and DCP, α SMA expression was found to terminate abruptly prior to reaching the DCP (inset I; black arrow). The locations of each vascular plexus are indicated in the retinal layers panel. **(B)** The DR- group showed additional α SMA expression along veins, venules, and capillaries on the venous aspect of the circulation. Compared to the control group, there was

more α SMA expression at venular junctions. In addition, α SMA expression along the *a1* arteriole spanned its entire course and extended into the DCP (inset II; *black arrow*). The DR+ group was characterized by microaneurysms and capillary dropout within the DCP (*asterisks*; inset III). Compared to the control and DR- groups, there was significantly more α SMA expression along veins, venules, and capillaries on the venous aspect. Within the DCP, α SMA expression was found distal to the *a1* arterioles and at venular junctions (inset III; *blue arrow*).

studies are required to determine if α SMA changes represent a compensatory mechanism⁵¹ that serves to increase oxygenation to regions of increased metabolic demand in the DCP or if they serve to propagate neuronal injury. The “no-reflow” mechanism has been observed following cardiac^{48,52,53} and cerebral ischemia,^{53,54} and it describes a phenomenon whereby abnormal and sustained capillary constriction due to pericytes overexpressing α SMA limits blood flow and propagates neuronal damage to an already ischemic region. A disease stage-specific increase in α SMA in the DCP suggests that a similar mechanism may be occurring in DR and may explain why the earliest ischemic changes in DR are seen within the DCP.^{55–57}

The occurrence of a significantly greater number of inflow pathways that directly connect retinal arteries to the ICP in preclinical DR and clinical DR eyes implicates the establishment of a “steal” effect in diabetes where blood flow is preferentially diverted from the SVP to the ICP and DCP. Kornfield and Newman¹⁷ demonstrated a similar physiologic “steal” effect in rat eyes using flicker stimulation that induced significantly greater dilation of intermediate layer capillaries than in capillaries of the superficial and deep vascular layers. The ICP supplies the neurons and synapses of the superficial portion of the inner nuclear layer and the deep portion of the inner plexiform layer, respectively.^{25,26} The preferential diversion of blood flow to the ICP may reflect a disproportionate increase in energy demands in these retinal compartments in diabetes.⁵⁸ We did not find a significant difference in the frequency of venous draining pathways between the control and DR groups, although there was a stage-specific increase in the degree of α SMA staining within elements of the venous circulation in DR. In our previous work, we showed that endothelia of the retinal veins have contractile properties, and retinal vein tone can be modulated by vasoactive factors such as endothelin-1 and adenosine.⁵⁹ The relevance of increased expression of α SMA in the retinal venous circulation in diabetes is twofold: (1) it implies that the venous circulation may play a critical role in modulating retinal blood flow changes in diabetes as a compensatory or pathologic mechanism; and (2) systemic or ocular therapies that target the vasoactive properties of the retinal circulation may be useful for reversing retinal vascular damage in diabetes.

In 1993, Cringle and colleagues⁶⁰ published a seminal report comparing retinal blood flow by hydrogen clearance polarography between streptozotocin-induced diabetic rats and controls. They demonstrated a 47% increase in mean retinal blood flow, as well as greater heterogeneity in retinal blood flow, characteristics after 5 to 6 weeks of experimentally induced diabetes. Retinal blood flow changes were observed prior to the occurrence of pathologic retinal vascular abnormalities. The current report provides a histologic basis for understanding these perfusion abnormalities and suggests that alterations in α SMA expression and arterial inflow pathways within the vascular tree may underlie retinal blood flow changes in diabetes. Recently we described a technique whereby analysis of successive algorithm-aligned optical coherence tomography angiography (OCTA) frames

can be used to derive a measure of spatial and temporal variations in human retinal perfusion.⁴³ With the increasing availability of OCTA technology it may be possible to harness such techniques to facilitate rapid and non-invasive detection of the earliest stages of DR before the onset of structural changes such as pericyte loss and the formation of microaneurysms.^{7,61,62}

Strengths of this study include the large sample size (total of 28 human donor eyes) and the precise quantitative evaluation of vascular parameters using high-resolution confocal scanning laser microscopy. Precise labeling of the retinal vasculature was also achieved using our well-established, perfusion-based antibody-labeling techniques that obviate many of the shortfalls associated with immersion tissue labeling and section labeling.⁶³ Collectively, these techniques permitted us to propose the sequences and interrelationships among α SMA expression, blood flow pathways, and capillary density alterations in the development of DR as summarized in Figure 9. We acknowledge that this study was limited by the investigation of only one vascular contractile protein— α SMA, the distribution of which was analyzed in a largely qualitative manner. The distribution and significance of other contractile proteins such as myosin and its isoforms remain to be elucidated.

Acknowledgments

The authors thank the staff of Western Australia Lions Eye Bank and DonateLife for facilitating the donor eye retrieval process.

Supported by a grant from the Investigator Grant of National Health and Medical Research Council of Australia (APP1173403).

Disclosure: **D. An**, None; **J. Chung-Wah-Cheong**, None; **D.-Y. Yu**, None; **C. Balaratnasingam**, None

References

1. Yanoff M. Diabetic retinopathy. *N Engl J Med*. 1966; 274(24):1344–1349.
2. Davis MD. Diabetic retinopathy. A clinical overview. *Diabetes Care*. 1992;15(12):1844–1874.
3. Frank RN. The galactosemic dog. A valid model for both early and late stages of diabetic retinopathy. *Arch Ophthalmol*. 1995;113(3):275–276.
4. Safi H, Safi S, Hafezi-Moghadam A, Ahmadi H. Early detection of diabetic retinopathy. *Surv Ophthalmol*. 2018;63(5):601–608.
5. Early Treatment Diabetic Retinopathy Study Research Group. Grading diabetic retinopathy from stereoscopic color fundus photographs—an extension of the modified Airlie House classification. ETDRS Report Number 10. *Ophthalmology*. 1991;98(5 suppl):786–806.
6. Hammes HP, Lin J, Renner O, et al. Pericytes and the pathogenesis of diabetic retinopathy. *Diabetes*. 2002;51(10):3107–3112.

7. Cogan DG, Toussaint D, Kuwabara T. Retinal vascular pattern. IV. Diabetic retinopathy. *Arch Ophthalmol*. 1961;66:366–378.
8. Ashton N. Studies of the retinal capillaries in relation to diabetic and other retinopathies. *Br J Ophthalmol*. 1963;47:521–538.
9. Pope CH, Jr. Retinal capillary microaneurysms: a concept of pathogenesis. *Diabetes*. 1960;9:9–13.
10. Yanoff M. Ocular pathology of diabetes mellitus. *Am J Ophthalmol*. 1969;67(1):21–38.
11. Yu D-Y, Cringle SJ. Oxygen distribution and consumption within the retina in vascularised and avascular retinas and in animal models of retinal disease. *Prog Retin Eye Res*. 2001;20(2):175–208.
12. Wangsa-Wirawan ND, Linsenmeier RA. Retinal oxygen: fundamental and clinical aspects. *Arch Ophthalmol*. 2003;121(4):547–557.
13. Hardarson SH, Basit S, Jonsdottir TE, et al. Oxygen saturation in human retinal vessels is higher in dark than in light. *Invest Ophthalmol Vis Sci*. 2009;50(5):2308–2311.
14. Yu DY, Cringle SJ, Su EN. Intraretinal oxygen distribution in the monkey retina and the response to systemic hyperoxia. *Invest Ophthalmol Vis Sci*. 2005;46(12):4728–4733.
15. Delaey C, Van De Voorde J. Regulatory mechanisms in the retinal and choroidal circulation. *Ophthalmic Res*. 2000;32(6):249–256.
16. Haefliger IO, Meyer P, Flammer J, Luscher TF. The vascular endothelium as a regulator of the ocular circulation: a new concept in ophthalmology? *Surv Ophthalmol*. 1994;39(2):123–132.
17. Kornfield TE, Newman EA. Regulation of blood flow in the retinal trilaminar vascular network. *J Neurosci*. 2014;34(34):11504–11513.
18. Trost A, Lange S, Schroedl F, et al. Brain and retinal pericytes: origin, function and role. *Front Cell Neurosci*. 2016;10:20.
19. Kim SJ, Kim SA, Choi YA, Park DY, Lee J. Alpha-smooth muscle actin-positive perivascular cells in diabetic retina and choroid. *Int J Mol Sci*. 2020;21(6):2158.
20. Yu PK, An D, Balaratnasingam C, Cringle SJ, Yu DY. Topographic distribution of contractile protein in the human macular microvasculature. *Invest Ophthalmol Vis Sci*. 2019;60(14):4574–4582.
21. Yemisci M, Gursoy-Ozdemir Y, Vural A, Can A, Topalkara K, Dalkara T. Pericyte contraction induced by oxidative-nitritative stress impairs capillary reflow despite successful opening of an occluded cerebral artery. *Nat Med*. 2009;15(9):1031–1037.
22. Burns SA, Elsner AE, Chui TY, et al. In vivo adaptive optics microvascular imaging in diabetic patients without clinically severe diabetic retinopathy. *Biomed Opt Express*. 2014;5(3):961–974.
23. Palochak CMA, Lee HE, Song J, et al. Retinal blood velocity and flow in early diabetes and diabetic retinopathy using adaptive optics scanning laser ophthalmoscopy. *J Clin Med*. 2019;8(8):1165.
24. Nesper PL, Roberts PK, Onishi AC, et al. Quantifying microvascular abnormalities with increasing severity of diabetic retinopathy using optical coherence tomography angiography. *Invest Ophthalmol Vis Sci*. 2017;58(6):BIO307–BIO315.
25. An D, Yu P, Freund KB, Yu DY, Balaratnasingam C. Three-dimensional characterization of the normal human parafoveal microvasculature using structural criteria and high-resolution confocal microscopy. *Invest Ophthalmol Vis Sci*. 2020;61(10):3.
26. Chan G, Balaratnasingam C, Yu PK, et al. Quantitative morphology of perifoveal capillary networks in the human retina. *Invest Ophthalmol Vis Sci*. 2012;53(9):5502–5514.
27. An D, Tan B, Yu DY, Balaratnasingam C. Differentiating microaneurysm pathophysiology in diabetic retinopathy through objective analysis of capillary nonperfusion, inflammation, and pericytes. *Diabetes*. 2022;71(4):733–746.
28. Yu PK, Mammo Z, Balaratnasingam C, Yu DY. Quantitative study of the macular microvasculature in human donor eyes. *Invest Ophthalmol Vis Sci*. 2018;59(1):108–116.
29. An D, Balaratnasingam C, Heisler M, et al. Quantitative comparisons between optical coherence tomography angiography and matched histology in the human eye. *Exp Eye Res*. 2018;170:13–19.
30. Schumacher U, Vischer P, Volker W, Engelmann B. Lectin binding and uptake and glycoprotein characterization of isolated porcine aortic endothelial and smooth muscle cells. *Cell Biochem Funct*. 1993;11(3):225–230.
31. Khoshnoodi J, Pedchenko V, Hudson BG. Mammalian collagen IV. *Microsc Res Tech*. 2008;71(5):357–370.
32. Nehls V, Drenckhahn D. Heterogeneity of microvascular pericytes for smooth muscle type alpha-actin. *J Cell Biol*. 1991;113(1):147–154.
33. Smyth LCD, Rustenhoven J, Scotter EL, et al. Markers for human brain pericytes and smooth muscle cells. *J Chem Neuroanat*. 2018;92:48–60.
34. Hughes S, Chan-Ling T. Characterization of smooth muscle cell and pericyte differentiation in the rat retina in vivo. *Invest Ophthalmol Vis Sci*. 2004;45(8):2795–2806.
35. Skalli O, Pelte MF, Peclet MC, et al. Alpha-smooth muscle actin, a differentiation marker of smooth muscle cells, is present in microfilamentous bundles of pericytes. *J Histochem Cytochem*. 1989;37(3):315–321.
36. Tan PE, Yu PK, Balaratnasingam C, et al. Quantitative confocal imaging of the retinal microvasculature in the human retina. *Invest Ophthalmol Vis Sci*. 2012;53(9):5728–5736.
37. Chan G, Balaratnasingam C, Yu PK, et al. Quantitative changes in perifoveal capillary networks in patients with vascular comorbidities. *Invest Ophthalmol Vis Sci*. 2013;54(8):5175–5185.
38. Chandrasekera E, An D, McAllister IL, Yu DY, Balaratnasingam C. Three-dimensional microscopy demonstrates series and parallel organization of human peripapillary capillary plexuses. *Invest Ophthalmol Vis Sci*. 2018;59(11):4327–4344.
39. Tuma RF, Durán WN, Ley K, eds. *Handbook of Physiology: Microcirculation*. 2nd ed. San Diego, CA: Academic Press; 2008.
40. Nesper PL, Soetikno BT, Zhang HF, Fawzi AA. OCT angiography and visible-light OCT in diabetic retinopathy. *Vision Res*. 2017;139:191–203.
41. Yu D-Y, Cringle SJ, Yu PK, Su E-N. Retinal energetics: its critical role in retinal physiology and pathology. *Expert Rev Ophthalmol*. 2011;6(4):395–399.
42. Ahmed J, Braun RD, Dunn R, Jr, Linsenmeier RA. Oxygen distribution in the macaque retina. *Invest Ophthalmol Vis Sci*. 1993;34(3):516–521.
43. Yu DY, Cringle SJ, Yu PK, et al. Retinal capillary perfusion: spatial and temporal heterogeneity. *Prog Retin Eye Res*. 2019;70:23–54.
44. Gabbiani G, Schmid E, Winter S, et al. Vascular smooth muscle cells differ from other smooth muscle cells: predominance of vimentin filaments and a specific alpha-type actin. *Proc Natl Acad Sci USA*. 1981;78(1):298–302.
45. Grant RI, Hartmann DA, Underly RG, Berthiaume A-A, Bhat NR, Shih AY. Classification of brain pericytes based on cell structure, location, and α -smooth muscle actin content. *bioRxiv*. 2017, <https://doi.org/10.1101/114777>.
46. Hill RA, Tong L, Yuan P, Murikinati S, Gupta S, Grutzendler J. Regional blood flow in the normal and ischemic brain is controlled by arteriolar smooth muscle cell contractility and not by capillary pericytes. *Neuron*. 2015;87(1):95–110.

47. Fernandez-Klett F, Offenhauser N, Dirnagl U, Priller J, Lindauer U. Pericytes in capillaries are contractile in vivo, but arterioles mediate functional hyperemia in the mouse brain. *Proc Natl Acad Sci USA*. 2010;107(51):22290–22295.
48. O'Farrell FM, Mastitskaya S, Hammond-Haley M, Freitas F, Wah WR, Attwell D. Capillary pericytes mediate coronary no-reflow after myocardial ischaemia. *eLife*. 2017;6:e29280.
49. Schmid-Schonbein H, Volger E. Red-cell aggregation and red-cell deformability in diabetes. *Diabetes*. 1976;25(2 suppl):897–902.
50. Roux E, Bougaran P, Dufourcq P, Couffignal T. Fluid shear stress sensing by the endothelial layer. *Front Physiol*. 2020;11(861):861.
51. Ostergaard L, Jespersen SN, Engedahl T, et al. Capillary dysfunction: its detection and causative role in dementias and stroke. *Curr Neurol Neurosci Rep*. 2015;15(6):37.
52. Rezkalla SH, Kloner RA. No-reflow phenomenon. *Circulation*. 2002;105(5):656–662.
53. Kloner RA, King KS, Harrington MG. No-reflow phenomenon in the heart and brain. *Am J Physiol Heart Circ Physiol*. 2018;315(3):H550–H562.
54. Ames A, 3rd, Wright RL, Kowada M, Thurston JM, Majno G. Cerebral ischemia. II. The no-reflow phenomenon. *Am J Pathol*. 1968;52(2):437–453.
55. An D, Pulford R, Morgan WH, Yu DY, Balaratnasingam C. Associations between capillary diameter, capillary density, and microaneurysms in diabetic retinopathy: a high-resolution confocal microscopy study. *Transl Vis Sci Technol*. 2021;10(2):6.
56. Furino C, Montrone G, Cicinelli MV, et al. Optical coherence tomography angiography in diabetic patients without diabetic retinopathy. *Eur J Ophthalmol*. 2020;30(6):1418–1423.
57. Kaizu Y, Nakao S, Arima M, et al. Capillary dropout is dominant in deep capillary plexus in early diabetic retinopathy in optical coherence tomography angiography. *Acta Ophthalmol*. 2019;97(5):e811–e812.
58. MacGregor LC, Rosecan LR, Laties AM, Matschinsky FM. Altered retinal metabolism in diabetes. I. Microanalysis of lipid, glucose, sorbitol, and myo-inositol in the choroid and in the individual layers of the rabbit retina. *J Biol Chem*. 1986;261(9):4046–4051.
59. Yu DY, Su EN, Cringle SJ, Morgan WH, McAllister IL, Yu PK. Local modulation of retinal vein tone. *Invest Ophthalmol Vis Sci*. 2016;57(2):412–419.
60. Cringle SJ, Yu DY, Alder VA, Su EN. Retinal blood flow by hydrogen clearance polarography in the streptozotocin-induced diabetic rat. *Invest Ophthalmol Vis Sci*. 1993;34(5):1716–1721.
61. Addison DJ, Garner A, Ashton N. Degeneration of intramural pericytes in diabetic retinopathy. *Br Med J*. 1970;1(5691):264–266.
62. Kuwabara T, Cogan DG. Retinal vascular patterns. VI. Mural cells of the retinal capillaries. *Arch Ophthalmol*. 1963;69:492–502.
63. Yu D. Isolated preparations of ocular vasculature and their applications in ophthalmic research. *Prog Retin Eye Res*. 2003;22(2):135–169.